Trapping of oxygen vacancy at grain boundary and its correlation with local atomic configuration and resultant excess energy in barium titanate: A systematic computational analysis

Takashi Oyama,* Nobuyuki Wada, and Hiroshi Takagi
Murata Manufacturing Co., Ltd., 10-1, Higashikotari 1-chome, Nagaokakyo-shi, Kyoto 617-8555, Japan

Masato Yoshiya
Department of Adaptive Machine Systems, Osaka University, 2-1, Yamadaoka, Suita-shi, Osaka 565-0871, Japan
(Received 7 October 2009; revised manuscript received 8 July 2010; published 6 October 2010)

Atomic structures of [001] symmetric tilt grain boundaries (GBs) and their influences on the trapping of oxygen vacancies at GBs in barium titanate ($BaTiO_3$) were analyzed using static atomistic simulation techniques. It is found that the structures are determined to minimize the deficiency in the coordination numbers of Ti^{4+} ions and to suppress the structural distortion in the vicinity of the GBs. The excess energy of the GB is dependent on the number density of the coordination-deficient Ti^{4+} ions, indicating that the ionic bonds between Ti^{4+} and O^{2-} ions are responsible for structural stabilization of GB. It is also found that the GB plays an important role in trapping oxygen vacancies, which acts as a resistance against the oxygen vacancy's diffusion. The trapping originates from the presence of irregular O^{2-} sites, where oxygen vacancies energetically prefer to reside, influenced by coordination environment. Based on the detailed analyses on origins of GB energy and the trapping in the vicinity of GB, new physical ground that correlates GB energy and capability of oxygen-vacancy trapping are provided, enabling us to predict how much vacancies can be trapped at GBs on the atomic level by micrometer-order measurement of GB energy. Electrical degradation of the $BaTiO_3$ dielectrics used for multilayer ceramic capacitors can be prevented through controlling the characteristics of the GBs to promote oxygen-vacancy trapping at GBs in polycrystalline materials via modifying materials synthesis procedures.

DOI: 10.1103/PhysRevB.82.134107 PACS number(s): 77.84.−s, 61.72.Mm, 68.35.Dv, 02.70.−c

I. INTRODUCTION

Barium titanate ($BaTiO_3$), which has a tetragonal perovskite structure at room temperature, is an invaluable material that is used in ceramic capacitors due to its high dielectric constant and low dielectric loss. $BaTiO_3$ used for multilayer ceramic capacitors (MLCCs) are cofired with nickel internal electrodes under low-oxygen partial pressure to prevent the oxidation of nickel. This brings about the formation of oxygen vacancies ($V_O^{\bullet\bullet}$) in sintered $BaTiO_3$ although sintered $BaTiO_3$ maintains insulator characteristics with the addition of divalent and/or trivalent dopants such as manganese and vanadium ions occupying Ti^{4+} sites.[1] The diffusion of $V_O^{\bullet\bullet}$ is activated at elevated temperatures by interchanges of $V_O^{\bullet\bullet}$ and O^{2-} between nearest-neighbor sites.[2] Under highly accelerated lifetime testing (HALT) imposing both thermal and dc electrical field stress, the $V_O^{\bullet\bullet}$ having positive effective charge in $BaTiO_3$ preferably diffuses toward the cathode, resulting in enrichment of the $V_O^{\bullet\bullet}$ near the cathode. The enrichment causes local electric field concentration at the interface between the $BaTiO_3$ dielectric and the cathode, resulting in electrical degradation of MLCCs.[3–5] Therefore, suppression of the diffusion is a significant issue in the development of dielectric materials for reliable MLCCs. Sakabe *et al.* showed that the degradation of MLCC is dramatically improved by the addition of rare-earth (*RE*) ions as donors into $BaTiO_3$.[6] Shirasaki *et al.* revealed that oxygen diffusivity of La-doped $BaTiO_3$ is lower than that of undoped $BaTiO_3$.[7] These phenomena originate from the trapping of $V_O^{\bullet\bullet}$ by cation vacancies associated with the doped RE^{3+} ions in the course of the diffusion.[8] However, further improvements of the degradation by the doping of RE^{3+} ions by experiment have become more difficult due to constraints including elemental species and amount of the doped RE^{3+} ions in light of controlling the dielectric properties.[9] To overcome this difficulty, other approaches, such as computational ones, are desired to develop $BaTiO_3$-based materials for more reliable MLCCs.

The dielectric materials used for MLCCs are polycrystalline ceramics and contain many grain boundaries (GBs). When the $V_O^{\bullet\bullet}$ in the $BaTiO_3$ ceramics migrates to the cathode under HALT conditions, the $V_O^{\bullet\bullet}$ is required to traverse many GBs. It has been reported that the diffusion behavior at the GB is different from that in the grain interior. According to Mann *et al.*, the reliability of an MLCC depends on the average number of grains per dielectric layer,[10] indicating that the GB in $BaTiO_3$ acts as a resistance against $V_O^{\bullet\bullet}$ diffusion. In contrast, Chazono *et al.*, based on results of impedance analyses, pointed out that the magnitude of GB resistivity is not large compared to the grain interior.[11] Although the influence of the GB on diffusion is still unclear, it is plausible to assume that GBs affect the overall diffusion property in polycrystalline $BaTiO_3$.

Recently, dielectric layers in MLCCs have been further thinned to acquire larger capacitance. The average size of grains has also been reduced to approximately 150 nm in diameter in the polycrystalline materials used for dielectric layers designed thinner than 1 μm.[12] The reduction in grain size increases the number of GBs per unit volume and, in turn, enhances the influence of GBs with respect to $V_O^{\bullet\bullet}$ diffusion. However, the lack of understanding regarding the role of the GBs for $V_O^{\bullet\bullet}$ diffusion impedes further improve-

ment and optimization of the reliability through controlling GB structures and their chemistry. Thus, a deeper understanding is required to realize advanced dielectric materials for more reliable MLCCs.

In this study, GB structures and interactions between the GB and $V_O^{\bullet\bullet}$ were investigated using static atomistic simulation techniques to reveal the correlation between the GB and atomistic mechanism for $V_O^{\bullet\bullet}$ diffusion in polycrystalline $BaTiO_3$. Various GBs, including $\Sigma 5$ (210), $\Sigma 5$ (310), $\Sigma 17$ (410), and $\Sigma 13$ (510)/[001] tilt GBs, were examined as model boundaries, and the interactions between each GB and $V_O^{\bullet\bullet}$ were analyzed in terms of the atomic structures and energies of the GBs. First, the structures and their resultant excess GB energies are quantitatively examined in Sec. III A. Then, the role of GBs for diffusion or trapping, and its structural dependence are discussed in Sec. III B through analyses of interaction energies between GBs and the $V_O^{\bullet\bullet}$.

II. COMPUTATIONAL PROCEDURE

A. Optimizations for grain-boundary structures

In order to find the atomistic mechanism by which $V_O^{\bullet\bullet}$ diffusion is suppressed or accelerated, structures, energies, and their correlations need to be accurately evaluated. Thus, it is rational to conduct static calculations rather than to perform dynamic simulation involving thermal fluctuations. Thus, lattice statics, rather than molecular dynamics, was employed as the computational method in this study. To obtain stable atomic GB structures, the energies of $BaTiO_3$ supercells containing the GBs were calculated by the lattice statics method using the GULP code.[13] In this method, optimal atomic positions as well as corresponding lattice energy can be obtained, and its availability has been verified in modeling $BaTiO_3$ with various point defects including $V_O^{\bullet\bullet}$.[14–16] In the case of an ionic compound, the lattice energy is given by a sum over all ionic pairs, which is partitioned into the long-range Coulombic and the short-range interaction parts. The Ewald method[17] was employed for the Coulombic part of the summation using the formal charges of barium, titanium, and oxygen ions of which values are +2, +4, and −2, respectively. The short-range interaction energy of an ionic pair was described by a Buckingham-type potential function, which is given by

$$\phi_{ij}(r_{ij}) = A_{ij}\exp\left(\frac{-r_{ij}}{\rho_{ij}}\right) - \frac{C_{ij}}{r_{ij}^6}, \tag{1}$$

where A_{ij}, ρ_{ij}, and C_{ij} are potential parameters for a pair of ions i and j, and r_{ij} is the distance between them. The potential parameters shown in Table I (Refs. 18–20) were used in this study. These parameters reproduce a cubic perovskite structure of a bulk $BaTiO_3$ model of which the lattice constant is 0.399 nm but fail to reproduce the tetragonal and monoclinic structures. However, this is a trivial problem in this study because HALT is commonly conducted at a temperature above 425 K, where a cubic structure is the most stable structure. Thus, it is reasonable to assume the cubic structure upon obtaining the GB structures that affect the $V_O^{\bullet\bullet}$ diffusion. The short-range interactions were truncated at r = 1 nm. All lattice statics calculations were performed under a constant volume condition to avoid numerical errors due to slight changes in supercell size and shape. Positions of all ions in the supercell were fully relaxed in the calculation to obtain optimized structure and its energy.

TABLE I. Short-range potential parameters for the Buckingham-type pairwise potential function used in this study.

Ion pair	A (eV)	ρ (10^{-2} nm)	C (10^{-6} eV nm^6)
O^{2-}-O^{2-}	9547.960[a]	2.1916[a]	32.000[a]
Ba^{2+}-O^{2-}	905.700[b]	3.9760[b]	0.000[b]
Ti^{4+}-O^{2-}	2179.122[c]	3.0384[c]	8.986[c]

[a]Reference 18.
[b]Reference 19.
[c]Reference 20.

A supercell including two identical GBs was used as the GB model in accordance with three-dimensional periodic boundary conditions. A schematic of a supercell is shown in Fig. 1. The lengths of the supercell edges and the number of ions in the supercells for the various GB models studied are summarized in Table II. The lattice constants of a unit cell that determine lengths of the supercell were fixed at 0.399 nm obtained from the static calculation for a unit cell of cubic $BaTiO_3$ under the constant pressure condition. The supercell length perpendicular to the GB plane a_{cell} was approximately 6 nm in all GB models. Thus, the GB planes in the supercell were separated by approximately 3 nm. It was verified, by preliminary calculations, that the interaction between the GBs is negligible small at the separation of 3 nm. The lengths of the two supercell edges parallel to the GB planes, namely, b_{cell} and c_{cell}, were one coincidence site lattice (CSL) unit-cell length and one perovskite unit-cell length, respectively. As shown in Fig. 2, in rigid-body translation (RBT) in the b_{cell} direction, the initial ion positions in one of the two grains were shifted with respect to the ideal positions generated by the CSL theory.[21] The initial RBT δ_b was given by

$$\delta_b = R_b b_{cell}, \tag{2}$$

where R_b is the initial RBT ratio, ranges from 0 to 1.0 with a

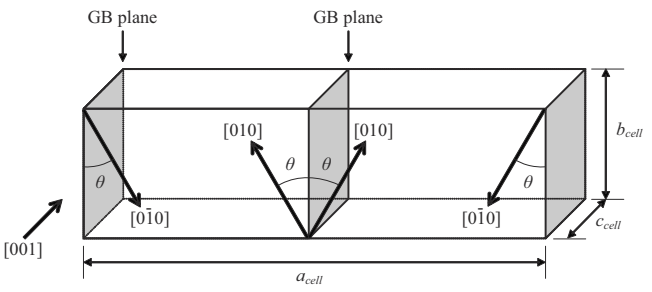

FIG. 1. Schematic of a supercell, where a_{cell}, b_{cell}, and c_{cell} are the lengths of the supercell edges. The misorientation angle 2θ between [010] directions of each crystal slab are listed in Table II with the supercell lengths.

TABLE II. Summary of the misorientation angles, the supercell lengths, and the number of ions contained in the supercells.

Boundary	Misorientation angle 2θ (deg)	Supercell lengths (nm)			Number of ions		
		a_{cell}	b_{cell}	c_{cell}	Ba^{2+}	Ti^{4+}	O^{2-}
Σ5 (210)	53.13	6.070	0.893	0.399	34	34	102
Σ5 (310)	36.86	6.060	1.262	0.399	48	48	144
Σ17 (410)	28.07	6.030	1.646	0.399	62	62	186
Σ13 (510)	22.62	6.107	2.036	0.399	78	78	234

0.05 step. In addition, two grains were separated by δ_a, ranging from 0.05 to 0.20 nm with a step of 0.001 nm. Therefore, the length of the supercell perpendicular to the GB plane was $a_{cell}+2\delta_a$ after the separation of the grains. The RBT in the c_{cell} direction was not taken into account in this study, since the RBT of this direction, thus far, to the authors' best knowledge, has not been experimentally or theoretically found at [001] tilt boundaries in cubic perovskites.[22,23]

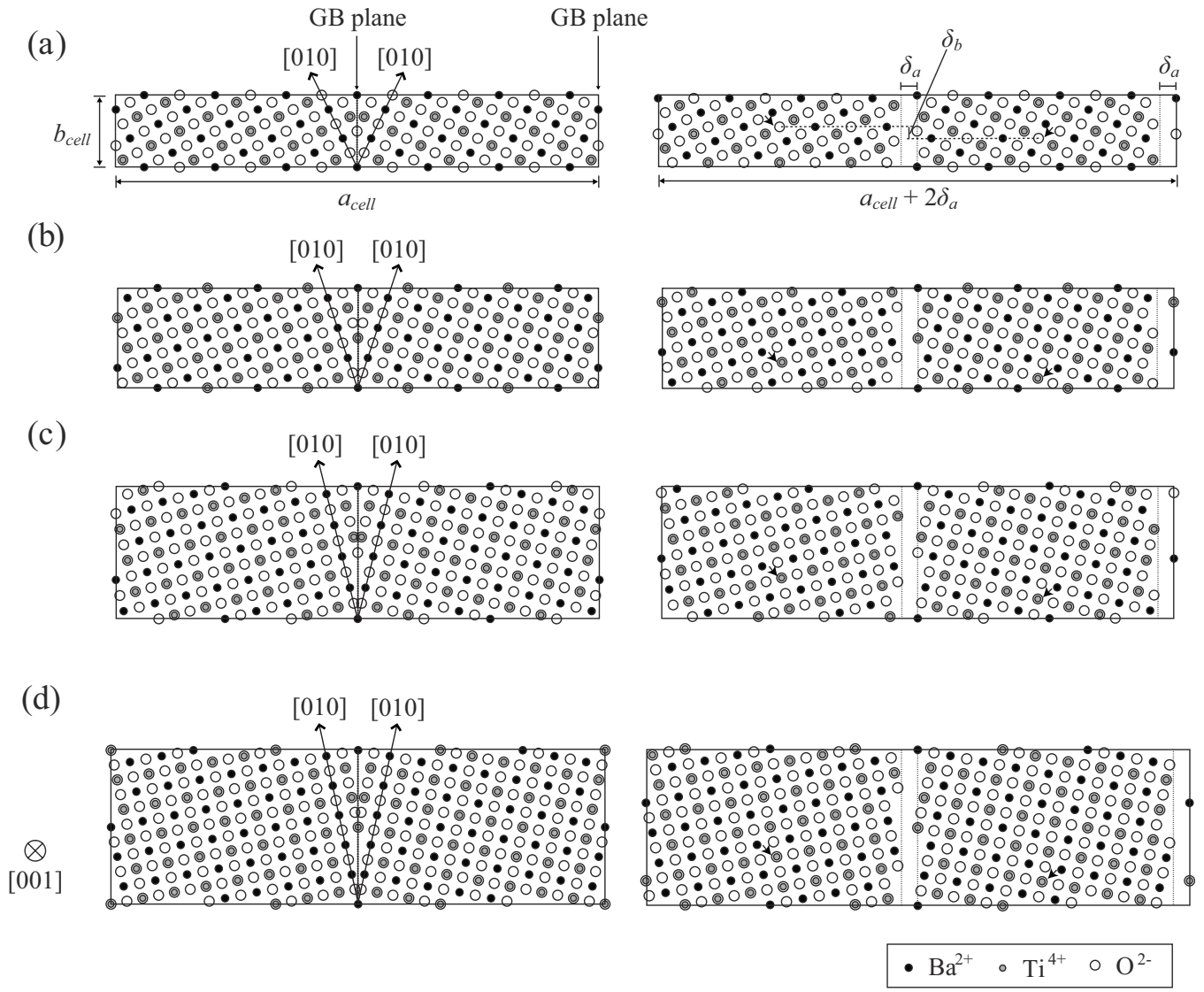

FIG. 2. Schematics of atomic configurations in the supercells viewed from [001] direction: (a) Σ5 (210), (b) Σ5 (310), (c) Σ17 (410), and (d) Σ13 (510) GB models. The left diagrams in the figure are the atomic configurations of perfect CSL boundaries. The right diagrams are the typical atomic configurations with the initial RBT δ_b and grain separation δ_a. O^{2-} ions, indicated by arrows, are used for evaluation of stable RBT after relaxation.

Excess energy, γ_{excess}, is an indicator of the stability of the GB structure, which is defined as

$$\gamma_{excess} = \frac{E_{\mathrm{GB}} - E_{bulk}}{2A}, \tag{3}$$

where A is the cross-sectional area of the GB plane in the supercell and E_{GB} is the lattice energy of the supercell containing two GBs. The lattice energy for a bulk model E_{bulk} was calculated from the bulk supercell with the same number of ions as that of the GB supercell. For a given misorientation of two adjoining grains, the excess energy changes with the RBT and the separation of two grains, δ_b and δ_a. When a specific set of RBT and grain separation yields minimal γ_{excess} for a given misorientation, it is referred to as GB energy, γ_{GB}, also defined by Eq. (3). The stable RBTs parallel to the b_{cell} direction and the excess volumes were evaluated in the respective stable GB structures. The value of the stable RBT along the b axis was measured by the difference in b components of the corresponding O^{2-} positions in the adjoining two grains (See Fig. 2). The excess volume V_{excess} was calculated from the volumes of the supercells,

$$V_{excess} = \frac{V_{\mathrm{GB}} - V_{bulk}}{2A}, \tag{4}$$

where V_{GB} and V_{bulk} are the volumes of the supercells of the GB and bulk models, respectively. Since the lengths of the supercell edges (i.e., $a_{cell}+2\delta_a$, b_{cell}, and c_{cell}) were fixed in the calculation under the constant volume condition, V_{excess} was equal to δ_a. The coordination numbers at Ba^{2+} and Ti^{4+} sites were also analyzed by counting the surrounding O^{2-} ions having distances from the nearest cation sites with cutoff values of 0.325 nm and 0.230 nm, respectively. These cutoff values were 1.15 times longer than the interionic distances between the cations and the nearest-neighbor O^{2-} ion in the perfect lattice.

B. Calculation for interaction energy between GB and $V_O^{\bullet\bullet}$

In the vicinity of the GB, atomic configuration deviates from that in the grain interior due to the lattice discontinuities at the GB and the resultant distortion leading to different coordination environments of the O^{2-} sites from those in the grain interior. Therefore, it is expected that an energy penalty due to substitution of a $V_O^{\bullet\bullet}$ for an O^{2-} ion differs between the GB region and the grain interior. This can be interpreted as an interaction between the GB and $V_O^{\bullet\bullet}$. The interactions act as a driving force for the trap or release of $V_O^{\bullet\bullet}$ at the GBs. In order to discuss the role of GB in $V_O^{\bullet\bullet}$ diffusion, the interaction energy, $E_{V_O\text{-GB}}$, was evaluated by

$$E_{V_O\text{-GB}}(r) = E_{def}(r) - E_{def}(\infty), \tag{5}$$

where E_{def} is the defect formation energy or substitution energy of a $V_O^{\bullet\bullet}$ for an O^{2-} ion, as a function of r, the distance of a $V_O^{\bullet\bullet}$ from the GB plane. Reference energy, $E_{def}(\infty)$, corresponds to the case where $V_O^{\bullet\bullet}$ is separated from the GB plane by infinite distance. The Mott-Littleton approximation[24,25] combined with the lattice statics method was used for the calculation of E_{def}. Although the Mott-Littleton method is not designed for the models containing GBs, it is reported that this method can be applied to defects at interface, as well as within the bulk of solid,[26] and that the energies of defects, such as oxygen vacancy, at interfaces including GBs were successfully analyzed in various oxides by employing this method.[27–31] Furthermore, it was verified, by preliminary calculations, that the energies as well as atomic coordinates obtained from various methods including the Mott-Littleton method are essentially unchanged irrespective of the methods employed if careful determination of calculation conditions are made in each method. For example, introduction of jellium-like uniform background charge to maintain charge neutrality instead of the Mott-Littleton method showed little difference according to our preliminary calculations. Thus, obtained results are not dependent on the Mott-Littleton method for GB models in this study. However, slight interaction between the defect and the periodically placed GBs remains when the Mott-Littleton method is used as well as the cases with other methods. To decrease the interaction, the longer supercell, with the length of approximately 10 nm in the a_{cell} direction, was used for the calculations of E_{def} in each GB model. In addition, to cancel out slight difference in the interactions between GB models, $E_{def}(r)$ obtained at $r=\sim 2.5$ nm (at the center of a grain in a GB supercell) was used as the reference energy in each GB model. In the calculations, spherical region I with a radius of 1.5 nm, in which all ion positions are relaxed in response to the centered $V_O^{\bullet\bullet}$, was assumed. Region IIa with a radius of 2.0 nm was also assumed to ensure a smooth transition between region I and the outer region.

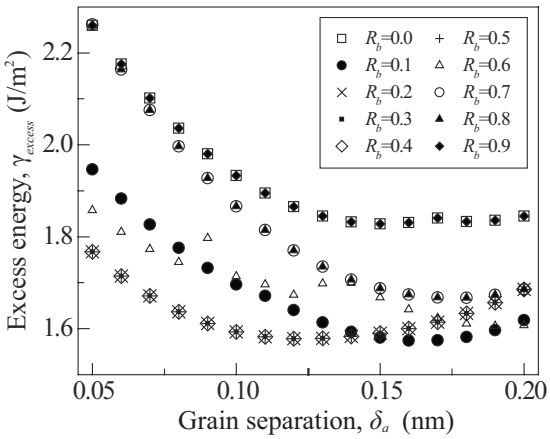

FIG. 3. Plots of γ_{excess} at each δ_b for $\Sigma 5$ (310) GB as a function of δ_a.

TABLE III. List of GB energies, RBTs, and excess volumes of the stable GB structures.

Boundary	GB energy (J/m^2)	RBT (nm)	Excess volume (nm)
$\Sigma 5$ (210)	1.034	<0.001	0.134
$\Sigma 5$ (310)	1.573	0.117	0.164
$\Sigma 17$ (410)	1.454	0.428	0.144
$\Sigma 13$ (510)	1.436	0.809	0.108

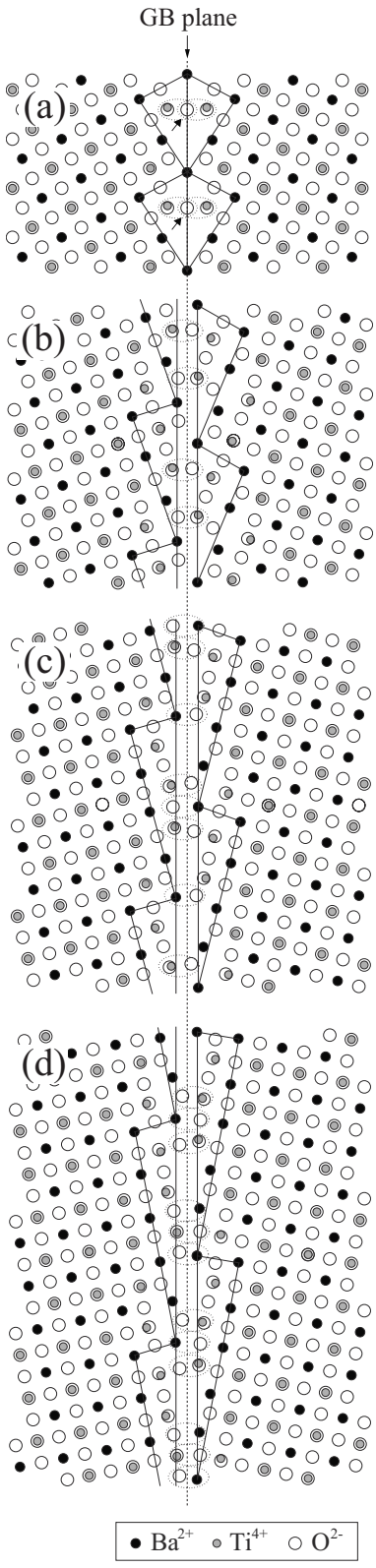

FIG. 4. Atomic configurations at the stable GBs viewed from [001] direction: (a) Σ5 (210), (b) Σ5 (310), (c) Σ17 (410), and (d) Σ13 (510) GBs. The dashed line is the adjoining GB plane. The triangles indicated by solid lines denote the structural units of the GBs defined in this study. The dotted circles indicate the ionic bonds across the GB planes. The arrows in Fig. 4(a) indicate O^{2-} ions which are displaced after relaxation.

It is known that Ti^{3+} ions are formed with oxygen vacancies when pure $BaTiO_3$ without any dopants is sintered under low-oxygen partial pressure.[32,33] However, formation of Ti^{3+} ions is suppressed in $BaTiO_3$ doped with manganese or vanadium ions occupying Ti^{4+} sites because positive effective charge due to oxygen vacancies is compensated by negative effective charge of the dopants.[1,34,35] Therefore, presence of Ti^{3+} ions was not taken into account in this study focusing on $BaTiO_3$ dielectrics for an application as MLCCs. Although the dopants remain at Ti^{4+} sites in $BaTiO_3$ lattice, presence of the dopants at Ti^{4+} sites were neglected to simplify the analysis of the interactions between GB and $V_O^{\bullet\bullet}$.

III. RESULTS AND DISCUSSIONS

A. Atomic structures and energies of GBs

Figure 3 shows γ_{excess} at each R_b, i.e., δ_b/b_{cell} for Σ5 (310) GB model as a function of δ_a. It is found that curve shapes differed depending on R_b while γ_{excess} smoothly changed with δ_a with a few exceptions. This means that the stable atomic configurations could be found in almost cases without being trapped at the metastable configurations when initial configurations given by δ_a and R_b. The data sets of γ_{excess} at $R_b=0.0$ and 0.9, 0.7 and 0.8, and 0.2–0.5 exhibited similar behaviors, respectively, indicating that the similar configurations were obtained after relaxations at R_b of these values, respectively. However, metastable configurations occasionally remained after relaxations. Exceptional data points, observed at $R_b=0.6$, are examples for those. In these cases, atomic configurations are obviously different from others and thus be easily sorted out. Molecular-dynamics simulation might help to eliminate these metastable configurations, though it is beyond the scope of this study. Accordingly, magnitudes of γ_{excess} and their changes can be clearly interpreted in terms of the atomic configurations obtained after relaxation. Similar results were also obtained in other GB models. These results indicate that taking into account both the RBT and grain separation is crucial in obtaining stable GB structures. The obtained GB energies γ_{GB} with the stable RBTs and excess volumes are listed in Table III and their respective atomic configurations are shown in Fig. 4. It was preliminarily verified that almost identical atomic configuration is obtained by the first-principles projector-augmented wave calculations with the generalized gradient approximation using VASP code[36–38] when the stable RBT and the excess volume are given to each GB model. The configuration of Σ5 (310) GB shown in Fig. 4(b) is also in good agreement with a high-angle annular dark field-scanning transmission electron microscopy (HAADF-STEM) image of Σ5 (310) GB in a $BaTiO_3$ bicrystal observed by Imaeda *et al.*[23] These support that our calculations identified the most stable GB structures based on γ_{GB}.

In $SrTiO_3$ perovskites, it has been suggested that some of the atomic columns parallel to the [001] are half filled at [001] tilt GBs to relieve local strain at the GBs.[39–42] However, the RBT and/or relaxation of ion positions were not sufficiently incorporated in the estimations of the GB structures in these studies. Our preliminary analysis of the excess energies showed that formations of the half-filled columns

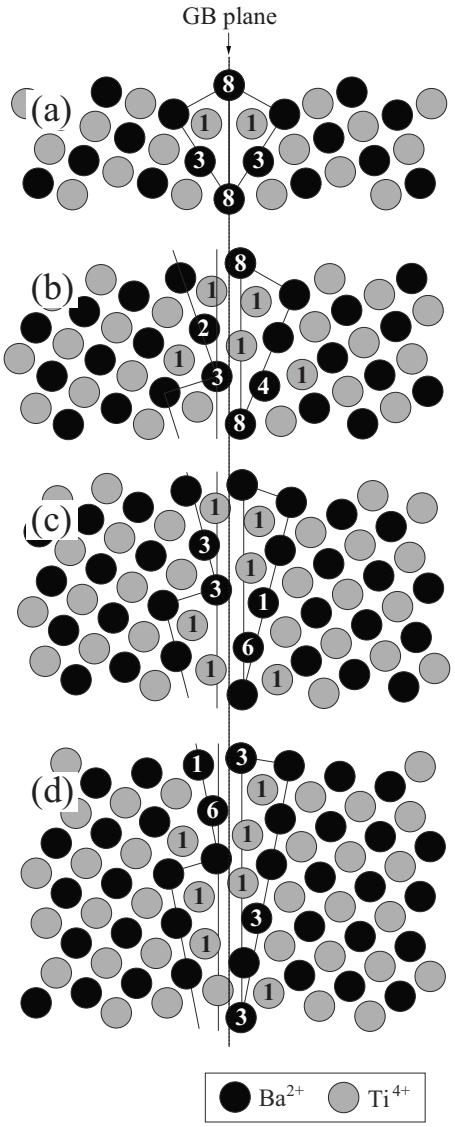

FIG. 5. The deficiency in the coordination of each cation site on the GBs: (a) Σ5 (210), (b) Σ5 (310), (c) Σ17 (410), and (d) Σ13 (510) GBs. The numbers written in the circles are the deficiency for the sites. The circles without the numbers denote perfect coordination.

are energetically unfavorable in all GB models. This is supported by the latest study of Σ5 (310) GBs of $SrTiO_3$ and $BaTiO_3$ incorporating RBT and relaxation with high accuracy.[23] Thus, the formations of the half-filled columns were not taken into account in this study.

The stable Σ5 (210) GB had a simple mirror symmetric structure because the RBT resulted simply in an increase in γ_{excess}. In contrast, the stable Σ5 (310), Σ17 (410), and Σ13 (510) GBs had mirror-glide symmetric structures due to the RBTs. When the triangular structural units dividing GB planes are defined, as shown in Fig. 4, it is recognized that the GB units in the Σ5 (210) GB are distorted, forming a kite-shaped structural unit and that the O^{2-} ions as indicated by arrows in Fig. 4(a) are displaced. In contrast, as shown in Figs. 4(b)–4(d), distortions of the GB units in the other GBs are smaller, almost the same as the atomic structure of the

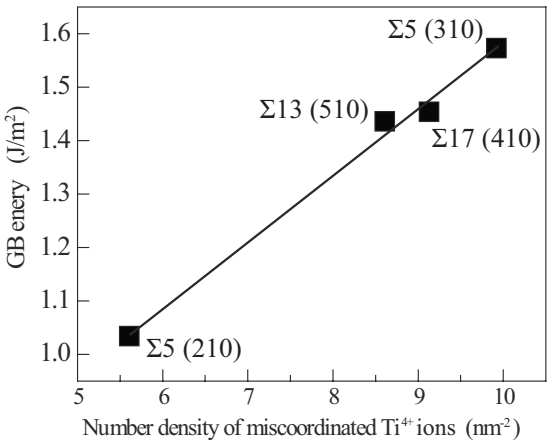

FIG. 6. Relationship between the number density of the coordination-deficient Ti^{4+} ions and the GB energy.

grain interior. These indicate that stable RBT effectively suppresses the distortion of the GB units to avoid the increase in local strain at the GB for smaller angle misorientation while formation of a kite-shaped distorted structural unit suppresses further distortion for larger angle misorientation. As shown in the left diagrams of Fig. 2, when some of ions with the same species are positioned close to each other across the GBs in mirror symmetry with the GB plane being the mirror plane, the repulsive force due to the Coulombic interaction would lead to the increase in energy and distortion of the GB unit because the volume in the GB region is expanded. In the case of Σ5 (310), Σ17 (410), and Σ13 (510) GBs with stable RBTs, grains are adjoined to the opposite ones, such that the ionic bonds are formed between the cation and the O^{2-} ion facing across the GB planes, as shown by dotted circles in Figs. 4(b)–4(d). As a result, the energy penalty due to the RBT is lower than that due to the kite-shaped distortion. The RBTs, therefore, are needed to reduce the energies of Σ5 (310), Σ17 (410), and Σ13 (510) GBs with the slightly modified GB units although the volumes in the GB regions are certainly expanded to retain reasonable bond lengths between cation and O^{2-} ion across the GB planes. In the case of Σ5 (210) GB, grains are adjoined without RBT and, therefore, formation of ionic bonds across the GB planes cannot be restored by RBT.

As mentioned above, ionic bonds across the GB planes are created upon the stable RBTs except for the Σ5 (210) GB. However, lattice discontinuities or dangling bonds remain at the GBs due to geometrical constraints, in part, represented by Σ values and indices of the adjoining GB planes. As a result, the coordination environments of the sites in the vicinity of the GB planes are different from those in the grain interior even after structural relaxation to minimize γ_{excess}. Figure 5 shows the deficiency in the coordination numbers of Ba^{2+} and Ti^{4+} ions on GBs. It is noted that perfect coordination numbers of Ba^{2+} and Ti^{4+} ions are 12 and 6, respectively. The deficiencies of Ba^{2+} ions on GBs ranged from 1 to 8 while Ti^{4+} ions on GBs exhibited deficiency of only 1 in all GB models, except for perfectly coordinated ions. These indicate that the atomic configurations at GBs with stable RBTs are relaxed to minimize the deficiencies of Ti^{4+} ions

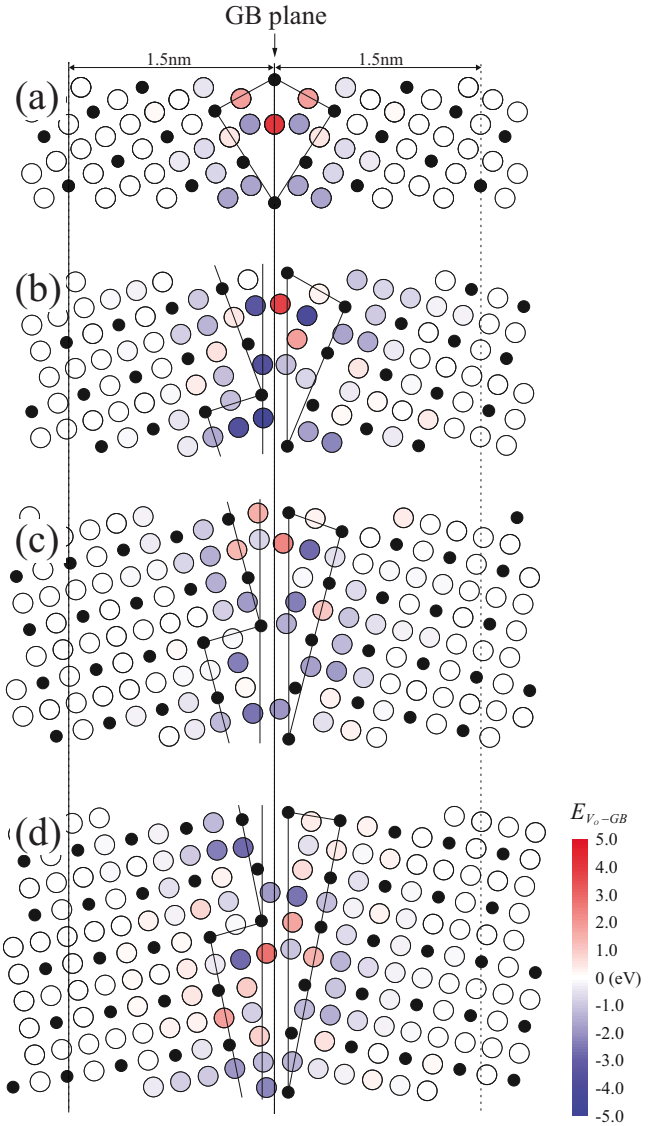

FIG. 7. (Color online) The magnitude of $E_{V_O\text{-GB}}$ at O^{2-} sites in the vicinity of the GBs: (a) Σ5 (210), (b) Σ5 (310), (c) Σ17 (410), and (d) Σ13 (510) GBs. Negative and positive values of $E_{V_O\text{-GB}}$ are represented by blue and red colors, respectively, as indicated by the scale bar at the right bottom side of the figure. The filled circles are the positions of Ba^{2+} ions.

rather than those of Ba^{2+} ions. There are two factors that affect Coulombic interaction between cations and O^{2-} ions: valence of the cation, which is twice as large for Ti^{4+} as for Ba^{2+}, and interionic distance, which is $\sqrt{2}$ times longer for Ba^{2+}-O^{2-} than for Ti^{4+}-O^{2-}. Taking these two factors into account, the Coulombic attractive force between Ti^{4+} and O^{2-} ions is larger than that between Ba^{2+} and O^{2-} ions in the $BaTiO_3$ lattice. This suggests that maintaining the coordination numbers of the Ti^{4+} ions by sacrificing those of Ba^{2+} ions is energetically more favorable for stable GBs. It can be perceived, therefore, that the ionic bonds between Ti^{4+} and O^{2-} ions at the GB dominantly stabilize the atomic structures of the GBs in $BaTiO_3$ while the ionic bonds between Ba^{2+} and O^{2-} ions contribute less to structural stabilization.

As shown in Fig. 5, the numbers of the coordination-deficient Ti^{4+} ions per unit area on the GB plane were different among the respective GB models. Figure 6 shows the relationship between the number density of the coordination-deficient Ti^{4+} ions per unit area and the GB energy. The GB energy linearly increased with increasing the number density. According to Shibata *et al.*, the GB energy is closely correlated with the density of the coordination-deficient Zr^{4+} ions at the GB in ZrO_2 fluorites.[43] This means that reduction in the Coulombic interactions between cation and anion due to the deficiency of the coordination numbers increases the GB energy in binary oxides. Even if composition and structure are different between these oxides, an origin governing the GB energy is identical in oxide ceramics including $BaTiO_3$. Besides, in the case of $BaTiO_3$, the linear relationship holds even when a deficiency in the coordination number of Ba^{2+} ions is neglected, suggesting that the contribution of Ba^{2+} coordination is rather small. As the Coulombic interaction between Ti^{4+} and O^{2-} ions is larger than that of Ba^{2+} and O^{2-} ions at the GBs, the accumulation of coordination-deficient Ti^{4+} ions at the GB mainly governs the excess energy of the stable GB in $BaTiO_3$.

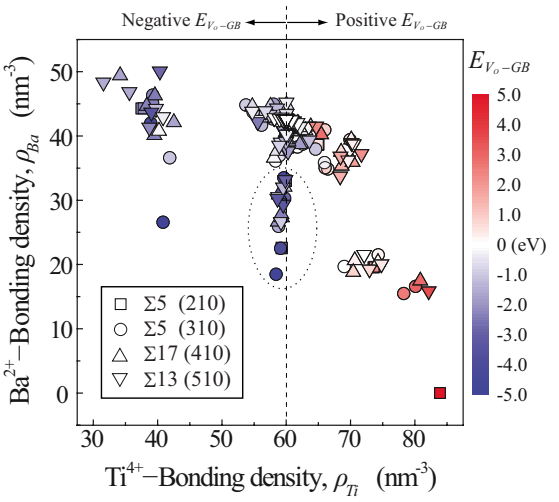

FIG. 8. (Color online) Scatter diagram for $E_{V_O\text{-GB}}$ in all GB models with ρ_{Ti} and ρ_{Ba} for horizontal and vertical axes, respectively. Negative and positive values of $E_{V_O\text{-GB}}$ are represented by blue and red colors, respectively. The dashed line indicates the coordination environment of Ti^{4+} ion in bulk. The data points indicated by dotted ellipse are the O^{2-} sites owning low ρ_{Ba} with bulk-like ρ_{Ti}.

B. Interactions between GBs and oxygen vacancy

Figure 7 shows $E_{V_O\text{-GB}}$ at each O^{2-} site in the vicinity of the stable GBs, represented by color tone. In all GB models, it is found that O^{2-} sites showing positive and negative energy were localized in the GB regions, within 1.5 nm from the GB planes, and that there were more O^{2-} sites showing negative energy than those showing positive energy in all GB models. Since a $V_O^{\bullet\bullet}$ preferably occupies the negative energy site, $V_O^{\bullet\bullet}$ migrating to the GB region by thermal and electrical fields would then reside at the negative site. Even if the $V_O^{\bullet\bullet}$ occupying the negative energy site attempts to interchange with an O^{2-} ion with higher $E_{V_O\text{-GB}}$, the driving force for

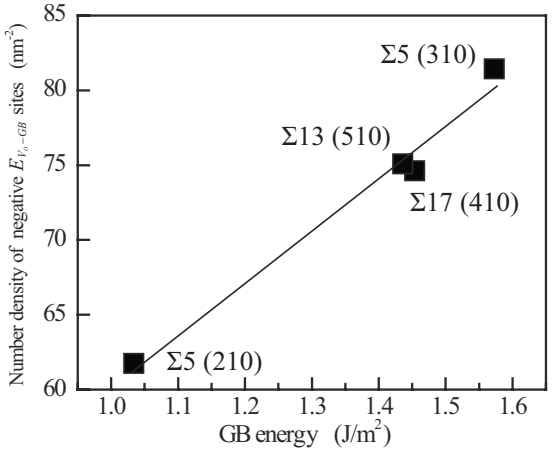

FIG. 9. GB energy dependence of the number density of the O^{2-} sites with negative $E_{V_O\text{-GB}}$ per unit area on the GB plane.

segregation into the negative energy site at GB region impedes the $V_O^{\bullet\bullet}$ diffusion away from the negative site. In other words, the $V_O^{\bullet\bullet}$ is trapped at the specific site in the GB region, resisting the diffusion of $V_O^{\bullet\bullet}$ beyond the GB region. Thus, the GB acts as a resistance against vacancy diffusion across the GB in $BaTiO_3$. On the other hand, the positive energy sites are periodically distributed along the GB plane according to periodicity of the GB structure. If a $V_O^{\bullet\bullet}$ trapped at the negative energy site attempts to migrate along GB, the $V_O^{\bullet\bullet}$ transiently needs to pass through the higher energy site in GB region. Then, the driving force for the segregation impedes further migration of the $V_O^{\bullet\bullet}$ along GB as is the case of the migration from the GB region back to grain interior. This means that the positive energy sites dotting in GB region impede the site interchanges although the $V_O^{\bullet\bullet}$ could repeat the interchanges between the sites with the similar $E_{V_O\text{-GB}}$. Consequently, the diffusion along GB is also suppressed as well as that across GB in the case of tilt GB. Further systematic study on twist GB is needed to generalize the findings, though it is beyond the scope of this study.

At the symmetric Σ5 (210) GB, the sites with similar interaction energies were symmetrically distributed on both sides of the GB as it is easily expected. In contrast, the distributions of the negative and positive energy sites were asymmetric at other GBs. Besides, changes in interaction energies with increasing distance from adjoining planes or in other directions were far from smooth in all GB models. These imply that local atomic configurations around the O^{2-} site, namely, coordination environments of the O^{2-} site, greatly affect the interaction between the GB and $V_O^{\bullet\bullet}$. However, the magnitude of the interaction energy could not be explained simply as a function of the cation coordination number of the O^{2-} site. Coordination distances to the cations are also important factors. To quantify these two factors in a combined form, the cation-bonding density of the O^{2-} site, $\rho_{cat.}$, is defined in order to evaluate the coordination environments including both the cation-coordination number and the coordination distance,

$$\rho_{cat.} = \sum_{i}^{CN_{cat.}} \left(\frac{4}{3}\pi r_i^3\right)^{-1}, \tag{6}$$

where $CN_{cat.}$ is the cation-coordination number for Ba^{2+} or Ti^{4+} ions and r_i is the distance to the cation. The $CN_{cat.}$ was evaluated in the same manner as for cations mentioned in the previous section. Figure 8 shows a scatter diagram for $E_{V_O\text{-GB}}$ in all GB models, with ρ_{Ti} and ρ_{Ba} for horizontal and vertical axes, respectively. The magnitude of $E_{V_O\text{-GB}}$ at each site is represented by the color tone in Fig. 8. The interaction energies exhibited negative values for $\rho_{Ti} < 60$ nm^{-3} in all GB models. In contrast, the interaction energies showed positive values for $\rho_{Ti} > 60$ nm^{-3} for most cases. The broken line at $\rho_{Ti} = 60$ nm^{-3} corresponds to that of the O^{2-} site in the grain interior, i.e., in a perfect crystal. These results indicate that the $V_O^{\bullet\bullet}$ tends to be trapped at the specific site of which the density of the surrounding Ti^{4+} ions is lower than that of the grain interior. Even if ρ_{Ti} were almost equal to 60 nm^{-3}, large magnitude of negative energy was found when ρ_{Ba} was less than 40 nm^{-3} as indicated by the dotted ellipse in Fig. 8. A decrease in the density of the surrounding Ba^{2+} ions barely affects the negative $E_{V_O\text{-GB}}$ and, in turn, the trapping of $V_O^{\bullet\bullet}$.

When an O^{2-} ion occupies this low Ti^{4+} density site, the Coulombic interactions between the O^{2-} and surrounding Ti^{4+} ions are smaller than those of the site in the grain interior. In contrast, the Coulombic interaction increases at the high Ti^{4+} density site. As shown in the previous section, the ionic bonds between O^{2-} and Ti^{4+} ions stabilize the GB structure by reducing excess energy. This means that an O^{2-} ion occupying a low Ti^{4+} density site increases the GB energy while an O^{2-} ion at a high Ti^{4+} density site decreases the GB energy. Replacing an O^{2-} ion with a $V_O^{\bullet\bullet}$ at a low Ti^{4+} density site, therefore, suppresses an increase in the GB energy relative to that in the grain interior. In contrast, $V_O^{\bullet\bullet}$ occupation of a high Ti^{4+} density site results in an increase in the GB energy. This is how $V_O^{\bullet\bullet}$ trapping sites and their distribution in the GB region are determined.

It is plausible that the magnitude of the GB energy is governed by the summation of the excess energies at the O^{2-} sites that represents interaction energy between O^{2-} ion and neighboring cations since the lattice energy is given as the summation of the potential energies of the O^{2-} sites in this study and interaction between cations is assumed to be zero with Coulombic interaction between cations being smaller due to longer interionic distance. Therefore, the number of negative energy sites for $V_O^{\bullet\bullet}$ can be correlated with GB energy. Figure 9 shows the GB energy dependence of the number density of the negative energy sites per unit area on the GB plane. As it is expected based on the above discussion, the number density increased almost linearly with increasing GB energy. According to the Gibbs theory,[44] chemical potential determines the local concentration of an impurity at an interface when the interface and bulk are in equilibrium. On the atomic level, the chemical potentials of the interface and bulk are related to the coordination environments of the impurity sites at the interface and in bulk, respectively.[45] In the case of $BaTiO_3$ including $V_O^{\bullet\bullet}$ at dilute concentration, the chemical potential of $V_O^{\bullet\bullet}$ in the GB region is lower than that

in the grain interior because of energy gain by the occupation of the negative energy site. When an increasing number of $V_O^{\bullet\bullet}$'s sequentially occupy the negative energy sites, the chemical potential in the GB region increases since the energy gain of the O^{2-} sites decreases due to the increase in repulsive Coulombic interactions between $V_O^{\bullet\bullet}$'s. Then, $V_O^{\bullet\bullet}$'s increase in the GB region until the chemical potential in the GB region becomes equal to that in the grain interior. Thus, maximal concentration of the trapped $V_O^{\bullet\bullet}$ in the GB region depends on the number density of the negative energy sites although all of their sites are not always occupied by the $V_O^{\bullet\bullet}$'s. It is plausible to conclude that availability for the trapping of $V_O^{\bullet\bullet}$ varies among different GBs and it depends on the GB energy determined by the atomic configurations in the vicinity of the GB. In other words, experimentally measurable GB energy is a micrometer-order indicator as to how much $V_O^{\bullet\bullet}$ can be trapped at GBs on the atomic level.

The above discussions lead to important predictions for dielectric material design for reliable MLCCs. The volume fraction of the GBs and, in turn, GB resistivity against the diffusion of $V_O^{\bullet\bullet}$ increases with the decreasing grain sizes in ceramics. In addition, the resistance can be enhanced by tailoring GBs regarding mismatching structures by low-temperature sintering just to densify without grain growth, for example. These are effective ways to suppress vacancy diffusion across GBs and, in turn, to prevent electrical degradation due to accumulation of $V_O^{\bullet\bullet}$ s near the cathode in dielectrics.

IV. CONCLUSIONS

Atomic structures of [001] tilt grain boundaries in $BaTiO_3$ and their interactions with oxygen vacancies were investigated by theoretical calculations using static atomistic simulation techniques. The following conclusions have been drawn in this study: (1) stable atomic configurations in the vicinity of the grain boundaries are determined such that deficiencies in the coordination numbers of Ti^{4+} ions are minimized, and the excess energy of the GB depends on the density of the coordination-deficient Ti^{4+} ions. Rigid-body translations of one grain with respect to the other occur at $\Sigma 5$ (310), $\Sigma 17$ (410), and $\Sigma 13$ (510) GBs in order to minimize the structural distortion in the vicinity of the GBs in addition to retaining the coordination numbers of Ti^{4+} ions as many as possible by sacrificing coordination numbers of Ba^{2+} ions.

(2) Grain boundaries attract oxygen vacancies, and trap them at specific sites of which local cation density is lower than that in the grain interior. Hence, grain boundaries act as a resistance for vacancy diffusion in polycrystalline $BaTiO_3$ ceramics. Amount and distribution of the trapping sites are closely related to the atomic structure of the GB and, in turn, GB energy, suggesting that the diffusion can be suppressed by controlling the GB structures with experimentally measurable GB energy as an indicator, in addition to increasing the volume fraction of the GBs or decreasing the grain size.

ACKNOWLEDGMENTS

The authors wish to thank K. Matsunaga of Kyoto University for his valuable discussions, and Y. Sakabe of the Murata Manufacturing Co., Ltd. for his continual advice and encouragement.

*Corresponding author; oyama@murata.co.jp

[1] I. Burn and G. H. Maher, J. Mater. Sci. **10**, 633 (1975).
[2] M. S. Islam, M. Cherry, and C. R. A. Catlow, J. Solid State Chem. **124**, 230 (1996).
[3] T. Baiatu, R. Waser, and K.-H. Härdtl, J. Am. Ceram. Soc. **73**, 1663 (1990).
[4] R. Waser, T. Baiatu, and K.-H. Härdtl, J. Am. Ceram. Soc. **73**, 1645 (1990).
[5] G. Y. Yang, E. C. Dickey, C. A. Randall, D. E. Barber, P. Pinceloup, M. A. Henderson, R. A. Hill, J. J. Beeson, and D. J. Skamser, J. Appl. Phys. **96**, 7492 (2004).
[6] Y. Sakabe, Y. Hamaji, H. Sano, and N. Wada, Jpn. J. Appl. Phys. **41**, 5668 (2002).
[7] S. Shirasaki, H. Yamamura, H. Haneda, K. Kakegawa, and J. Moori, J. Chem. Phys. **73**, 4640 (1980).
[8] T. Oyama, N. Wada, and Y. Sakabe, Key Eng. Mater. **388**, 269 (2009).
[9] Y. Hamaji, H. Sano, H. Wada, and K. Tomono, in *Proceedings of the Seventh US-Japan Seminar on Dielectric and Piezoelectric Ceramics*, Tsukuba, Japan, 14–17 November 1995, Tsukuba, Japan, IV-5, 273 (1995).
[10] L. Mann, M. Randall, D. Barber, P. Pinceloup, J. Beeson, G.-Y. Yang, and E. Dickey, *Program Summary and Extended Abstract of the 11th US-Japan Seminar on Dielectric and Piezoelectric Ceramics*, 2003, Vol. 39.
[11] H. Chazono and H. Kishi, Jpn. J. Appl. Phys. **40**, 5624 (2001).
[12] N. Wada, H. Tanaka, Y. Hamaji, and Y. Sakabe, Jpn. J. Appl. Phys. **35**, 5141 (1996).
[13] J. D. Gale, J. Chem. Soc., Faraday Trans. **93**, 629 (1997).
[14] G. V. Lewis and C. R. A. Catlow, Radiat. Eff. **73**, 307 (1983).
[15] G. V. Lewis, C. R. A. Catlow, and R. E. W. Casselton, J. Am. Ceram. Soc. **68**, 555 (1985).
[16] G. V. Lewis and C. R. A. Catlow, J. Phys. Chem. Solids **47**, 89 (1986).
[17] P. P. Ewald, Ann. Phys. **369**, 253 (1921).
[18] R. W. Grimes, D. J. Binks, and A. B. Lidiard, Philos. Mag. A **72**, 651 (1995).
[19] G. Busker, A. Chroneos, R. W. Grimes, and I.-Wei Chen, J. Am. Ceram. Soc. **82**, 1553 (1999).
[20] M. A. Mccoy, R. W. Grimes, and W. E. Lee, Philos. Mag. A **75**, 833 (1997).
[21] M. L. Kronberg and F. H. Wilson, Trans. Am. Inst. Min., Metall. Pet. Eng. **185**, 501 (1949).
[22] M. M. McGibbon, N. D. Browning, M. F. Chisholm, A. J. McGibbon, S. J. Pennycook, V. Ravikumar, and V. P. Dravid, Science **266**, 102 (1994).

[23] M. Imaeda, T. Mizoguchi, Y. Sato, H.-S. Lee, S. D. Findlay, N. Shibata, T. Yamamoto, and Y. Ikuhara, Phys. Rev. B **78**, 245320 (2008).
[24] N. F. Mott and M. J. Littleton, Trans. Faraday Soc. **34**, 485 (1938).
[25] C. R. A. Catlow, J. Chem. Soc., Faraday Trans. **85**, 335 (1989).
[26] V. E. Henrich and P. A. Cox, *The Surface Science of Metal Oxides* (Cambridge University Press, Cambridge, England, 1996), p. 23.
[27] D. M. Duffy, J. P. Hoare, and P. W. Tasker, J. Phys. C **17**, L195 (1984).
[28] M. S. Islam, D. J. Ilett, and S. C. Parker, J. Phys. Chem. **98**, 9637 (1994).
[29] C. R. A. Catlow, P. S. Baram, S. C. Parker, J. Purton, and K. V. Wright, Philos. Trans. R. Soc. London **350**, 265 (1995).
[30] M. S. D. Read, M. S. Islam, G. W. Watson, F. King, and F. E. Hancock, J. Mater. Chem. **10**, 2298 (2000).
[31] Y. Sato, T. Yamamoto, and Y. Ikuhara, J. Am. Ceram. Soc. **90**, 337 (2007).
[32] F. A. Kröger and H. J. Vink, in *Solid State Physics*, edited by F. Seitz and D. Turnbull (Academic Press, New York, 1956), Vol. 307.
[33] J. H. Herbert, Trans. Br. Ceram. Soc. **62**, 645 (1963).
[34] Y. Sakabe, K. Minami, and K. Wakino, Jpn. J. Appl. Phys. **20**, 147 (1981).
[35] K. Kishi, S. Murai, H. Chazono, M. Oshio, and N. Yamaoka, Jpn. J. Appl. Phys. **26**, 1394 (1987).
[36] G. Kresse and J. Furthmuller, Phys. Rev. B **54**, 11169 (1996).
[37] J. P. Perdew, K. Burke, and M. Ernzerhof, Phys. Rev. Lett. **77**, 3865 (1996).
[38] G. Kresse and D. Joubert, Phys. Rev. B **59**, 1758 (1999).
[39] N. D. Browning, S. J. Pennycook, M. F. Chisholm, M. M. McGibbon, and A. J. McGibbon, Interface Sci. **2**, 397 (1995).
[40] N. D. Browning and S. J. Pennycook, J. Phys. D **29**, 1779 (1996).
[41] V. P. Dravid and V. Ravikumar, Interface Sci. **8**, 177 (2000).
[42] V. Ravikumar, V. P. Dravid and D. Wolf, Interface Sci. **8**, 157 (2000).
[43] N. Shibata, F. Oba, T. Yamamoto, and Y. Ikuhara, Philos. Mag. **84**, 2381 (2004).
[44] N. Ma, S. A. Degia, and Y. Wang, Acta Mater. **51**, 3687 (2003).
[45] T. Oyama, M. Yoshiya, H. Matsubara, and K. Matsunaga, Phys. Rev. B **71**, 224105 (2005).